Optical Materials 174 (2026) 117945

Contents lists available at ScienceDirect

Optical Materials

journal homepage: www.elsevier.com/locate/optmat

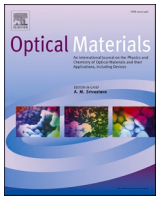

Research Article

Study of ZnS:Ag and $BaMgAl_{10}O_{17}:Eu^{2+}$ phosphor for UV-to-PAR spectral conversion greenhouse coatings

Chun-Ting Cho *, Erik van der Kolk

Luminescence Materials Group, Delft University of Technology, Mekelweg 15, Delft, the Netherlands

ARTICLE INFO

Keywords:
Hemispherical light transmittance
Greenhouse covering materials
Spectral conversion
Host absorption
Activator absorption

ABSTRACT

Spectral conversion films and coatings based on photoluminescent materials have attracted increasing attention for greenhouse applications and are reported to provide a net benefit through spectral control. However, there is little experimental data on spectral conversion coating that quantifies their optical properties, including absorption, transmittance, scattering loss, and the influence of the phosphor intrinsic parameters. In this work, UV-to-PAR spectral conversion coatings based on two commercial phosphors ZnS:Ag and $BaMgAl_{10}O_{17}:Eu^{2+}$ (BAM:Eu), with different particle loading and thickness, were fabricated and assessed by direct transmittance, hemispherical light transmittance (T_{HEM}), and diffuse reflectance. Transmittance decreased with increasing coating thickness and particle loading, whereas backward scattering showed the opposite trend. Performance indicators derived from direct transmittance revealed that host-absorption ZnS:Ag coatings exhibited greater UV absorption and higher PAR Enhancement than activator-absorption BAM:Eu coatings, resulting from their higher absorption coefficient. Quantum yield had a minimal impact because both phosphors displayed close PLQY values. However, the backward scattering of ZnS:Ag coatings was more pronounced than that of BAM:Eu coating due to the high refractive index of ZnS:Ag ($n \approx 2.3$), as confirmed by diffuse reflectance measurements. The 18 mass%, 200 μm ZnS:Ag coating showed the highest 1.3% PAR Enhancement, but its T_{HEM} was reduced by about 45%, demonstrating that backward scattering can counteract the benefits of spectral conversion. A general discussion for phosphor selection in greenhouse applications is also provided in this work.

1. Introduction

Food insecurity currently affects hundreds of millions of people worldwide [1,2]. Greenhouses are emerging as a critical solution offering reduced reliance on weather conditions and significantly higher crop yields per unit area compared to traditional open-field agriculture [3–5]. With the advancement of greenhouse technology, interest in innovative greenhouse roofs featuring functionalities such as scattering, anti-reflection, and spectrum shifting has grown rapidly over the past decade [6–16].

A growing number of research articles on spectral conversion greenhouse covers are published each year. Fan et al. provided a comprehensive overview of spectral conversion strategies (i.e., down-converting high-energy radiation to lower-energy radiation) and the phosphor materials suitable for each approach, and discussed the potential economic benefits of deploying luminescent conversion films for crop yield enhancement [17]. UV radiation constitutes 7 - 10% of the solar spectrum relative to photosynthetically active radiation (PAR, 400 - 700 nm), depending on air mass and weather conditions [18]. UV is often considered detrimental to crops because it can damage plant cells and is therefore typically absorbed or reflected by greenhouse roofs [19–21]. Following the generally accepted rule that "1% extra light can lead to 1% extra crop yield", greenhouse production can be increased if UV radiation is efficiently converted to PAR [22,23]. Shabalina et al. reviewed photoconversion cover (PCC) developments from 2020 to 2024 and summarized various greenhouse test outcomes across 58 PCC studies [24]. Although greenhouse studies increasingly report yield gains from spectral conversion covers, quantitative characterization of the cover's optical properties and accompanying optical trade-offs, particularly PAR losses arising from reduced transmittance and enhanced backward scattering, remains limited [24,25].

In this work, we present the next stage in the development of "UV-to-PAR" solar spectral conversion phosphor coatings for greenhouse applications by fabricating commercially viable spray-on coatings with varying thicknesses and particle mass loadings, and systematically characterizing the coating's optical properties. Using three different

* Corresponding author.
E-mail address: c.cho@tudelft.nl (C.-T. Cho).

https://doi.org/10.1016/j.optmat.2026.117945
Received 11 December 2025; Received in revised form 14 January 2026; Accepted 5 February 2026
Available online 6 February 2026

integrating sphere setups, we measured photoluminescence, diffuse reflectance, perpendicular transmittance, and hemispherical light transmittance (T_{HEM}). From these measurements, we determined key optical properties relevant for greenhouse applications, including the photoluminescence quantum yield (PLQY), UV absorption, UV-to-PAR conversion efficiency, and PAR Enhancement. This study quantifies both the gains and losses associated with such coatings by examining a set of commercially available UV-absorbing, PAR-emitting phosphors, namely ZnS:Ag and $BaMgAl_{10}O_{17}:Eu^{2+}$. We investigate how coating performance correlates with intrinsic material properties such as quantum yield, refractive index, and absorption strength (by the doping ions or the host matrix). This work is intended as a practical reference for greenhouse stakeholders and materials developers. By presenting fundamental optical metrics, this study provides guidance for selecting appropriate phosphors for specific performance objectives.

2. Material and methodology

2.1. Coating preparation

2.1.1. Selected phosphor

One host-absorption phosphor ZnS:Ag and one activator-absorption phosphor $BaMgAl_{10}O_{17}:Eu^{2+}$ (BAM:Eu) were purchased from Phosphor Technology. The dopant content of Eu^{2+} is 0.35 mol%. The dopant content of Ag is too little to be detected by scanning electron microscope, but the emission property and supplier confirms the existing of Ag dopant in the ZnS phosphor. The mean particle size, provided by the supplier, is 4.1 μm for BAM:Eu and 8 μm for ZnS:Ag. The density of the phosphor is 4.0 g/cm^3 for ZnS:Ag, and 3.7 g/cm^3 for BAM:Eu. The refractive index (n) is 1.7 for BAM:Eu, and 2.3 for ZnS:Ag. The theoretical absorption coefficient at 340 nm is approximately $10^4 \sim 10^5$ cm^{-1} for ZnS and $10^3 \sim 10^4$ cm^{-1} for 1 mol% Eu^{2+} in oxide host [26,27]. The photoluminescence quantum yield (PLQY) of the two phosphors was characterized using a 340 nm LED and an integrating sphere. BAM:Eu and ZnS:Ag exhibited high PLQY values of 92% and 86%, respectively.

ZnS:Ag is used here primarily as a host-absorption benchmark because it combines strong UV absorption with a PLQY comparable to BAM:Eu, allowing a controlled comparison between host-absorption and activator-absorption phosphors. We note that ZnS host can darken under prolonged UV exposure due to photo-oxidation/defect formation [28]. Stabilization strategies (e.g., surface passivation/coatings and dopant/defect engineering) are therefore essential for long-term deployment.

2.1.2. Luminescent coating's formulation

The luminescent coating consists of a dispersing agent, defoamer, acrylic resin, thickeners, and the selected phosphor. The loading of phosphors are 9 mass% and 18 mass%. The applied wet thickness of coating were 50, 100, 150, 200 μm on a 1 mm thick fused silica substrate by a bar-coater (TQC film applicator, Industrial Physics). A batch of coatings with the same wet thicknesses but without the addition of phosphor was produced following the same recipe, which are referred to as “no-phosphor coatings”. All the results will be presented using the wet thickness values. The dry thickness measured by a profilometer (Dektak 8, Bruker), which are typically 4 times smaller than the wet thickness, is presented in the Appendix.

Because ZnS:Ag has a larger mean particle size than BAM:Eu, dispersion uniformity and mechanicalproperty impacts (e.g., flexibility and tensile strength) may differ in practical film processing. These particle–host compatibility aspects, including dispersion stability and mechanical testing, are outside the scope of the present optical benchmarking study and therefore not addressed in the work.

2.2. Characterization methodology

2.2.1. Photoluminescence and photoluminescence excitation measurement

The photoluminescence emission (PL) and excitation (PLE) spectra of the phosphors were recorded by a photomultiplier tube (R7600U-20, Hamamatsu) connected to a monochromator (SP2300, Princeton Instruments). A xenon lamp connected to another monochromator (Gemini 180, HORIBA) was used as an excitation light source. The photoluminescence spectrum of both phosphors were recorded under excitation of 340 nm light. The photoluminescence excitation spectrum was recorded by monitoring emission at 450 nm and corrected for the lamp spectrum intensity by a calibrated silicon diode.

2.2.2. UV-to-PAR performance indicators

The UV-to-PAR performance indicators quantify the luminescent coating's capability of converting UV to additional PAR. These indicators include coating's absorption spectrum $A_{coating}(\lambda)$ (%), UV-to-PAR conversion efficiency $\eta_{coating}$ (%), and PAR Enhancement (%). $\eta_{coating}$ in short is the number of emitted PAR photons entering the greenhouse per absorbed UV photon. PAR Enhancement equals the ratio of luminescence-generated PAR photons entering the greenhouse to the total PAR photons in the AM1.5 solar spectrum. The detailed characterization methodology is described in our previous work [23]. $A_{coating}(\lambda)$ and $\eta_{coating}$ of the luminescent coating in the UV region were determined using a direct transmittance system with a deuterium lamp (AvaLight-DH-S, Avantes) as the light source. The transmitted light spectra of a fused-silica substrate ($I_{substrate}(\lambda)$) and the luminescent coating on the substrate ($I_{coating}(\lambda)$) were collected by a spectrometer (QE65Pro, Ocean Optics) connected with an optical fiber (FC-UVIR600, Avantes) to an integrating sphere located behind the sample. This detection system was calibrated with a calibrated deuterium light source (UV40, Optronic Laboratories) and tungsten light source (EV81, EPLAB). $A_{coating}(\lambda)$ and $\eta_{coating}$ are defined as follows:

$$A_{coating}(\lambda) = 1 - \frac{I_{coating}(\lambda)}{C_{Ref} * I_{substrate}(\lambda)} \tag{1}$$

$$\eta_{coating} = \frac{\int_{400}^{700} \left[I_{coating}(\lambda) - C_{Ref} * I_{substrate}(\lambda)\right] d\lambda}{\int_{250}^{400} \left[C_{Ref} * I_{substrate}(\lambda) - I_{coating}(\lambda)\right] d\lambda} \tag{2}$$

$I_{coating}(\lambda)$ and $I_{substrate}(\lambda)$ are the transmitted signals collected by an integrating sphere. In our measurement configuration, the following equation holds: $1 = A + T + R + W$, in which W equals the waveguided fraction escaping through the sample edges. Although we measured the backward reflection R (through diffuse reflectance measurement) and transmission T, we cannot reliably measure W. Therefore, we have introduced a more practical and reliable metric C_{Ref} that takes into account the influence of both the backward scattering and waveguiding effects on the loss of incident PAR photon flux. C_{Ref} was determined within a near-infrared (NIR) spectral range, 700 - 750 nm, unaffected by both emission and absorption. By applying C_{Ref}, the influence of backward scattering and waveguiding effects (R + W) can be removed from the calculations of $A_{coating}(\lambda)$ and $\eta_{coating}$. An assumption of constant backward scattering and waveguiding effects between 250 and 900 nm was made.

The PAR Enhancement was subsequently calculated using $A_{coating}(\lambda)$ and $\eta_{coating}$ according to

$$PAR\ enhancement = \frac{\eta_{coating} * \int_{250}^{400} \left[A_{coating}(\lambda) * I_{solar}(\lambda)\right] d\lambda}{\int_{400}^{700} I_{solar}(\lambda) d\lambda} \tag{3}$$

in which the integration part on the right hand side of this equation eliminates the influence of the lamp spectrum as if the measurements was done with the solar spectrum. The AM1.5 solar spectrum, $I_{solar}(\lambda)$, expressed in number of photons, was derived from the ASTM G173-03 Reference Spectra [29].

2.2.3. Hemispherical light transmittance

The hemispherical light transmittance T_{HEM} of all the coated samples was measured by a tabletop characterization system developed in Chapter 3. The calculation of T_{HEM} considers the wavelength range from 400 nm to 700 nm (PAR). A detailed description of the measurement procedure and calculation can be found in the cited work. Note that the T_{HEM} system employs a tungsten lamp as the light source, which emits mainly within the PAR region. Consequently, the obtained T_{HEM} values reflect not only PAR transmittance but also account for the absorption of blue photons and emission of red photons. The T_{HEM} of 1 mm-thick fused silica substrate was measured to be 87.7%.

2.2.4. Diffuse reflectance

The diffuse reflectance of all samples was measured using an integrating sphere (IS2004, Thorlabs) and in combination with a deuterium light source (AvaLight-DH-S, Avantes). The integrating sphere was positioned directly above the coating sample to collect the backward scattered (reflected) light (R) signals from the incident deuterium illumination. A reference measurement was obtained using the same reflective material as the inner surface of the integrating sphere. The diffuse reflectance of all coatings was measured by taking the average value in the NIR wavelength range (700 - 750 nm), where no absorption and emission occurred. The diffuse reflectance of 1 mm-thick fused silica substrate was measured to be 8.0%.

3. Results and discussions

The final appearance of the coating samples is presented in Figs. 1 and 2.

3.1. Photoluminescence excitation (PLE) and photoluminescence (PL) spectra

The photoluminescence excitation (PLE) and photoluminescence (PL) spectra of the selected phosphors are shown in Fig. 3. The absorption and emission mechanism of BAM:Eu originates from the activator ions, Eu^{2+}, characterized by the electronic transition from the ground state $4f^7$ to the excited state $4f^6 5\,d^1$. The two excitation peaks at 250 nm and 310 nm arise from the crystal field splitting of the 5d configuration. A broad emission peak at 450 nm is a distinctive feature of Eu^{2+} luminescence [30,31]. ZnS:Ag phosphor exhibited a sharp peak at 340 nm in the PLE spectrum corresponding to the band gap of ZnS (3.6 eV). The blue emission peak at 450 nm arises from electron-hole recombination after bandgap excitation from the valence band (VB) to the conduction band (CB), involving radiative relaxation via an intermediate energy level created by Ag^+ dopants located just above the VB of ZnS [32,33].

3.2. UV-to-PAR performance indicators

PAR Enhancement quantifies how much extra PAR light in the form of luminescence is entering the greenhouse due to UV absorption. Its efficiency is therefore a crucial quantity for UV-to-PAR type spectral conversion greenhouse coating. As explained in the methodology section, PAR Enhancement is derived from the coating's correction factor C_{Ref}, absorption spectrum $A_{coating}(\lambda)$, and UV-to-PAR conversion efficiency $\eta_{coating}$ of the coating. The influence of these quantities on PAR Enhancement is discussed in the following section.

Fig. 4 shows the transmittance spectra of all luminescent coatings ($I_{coating}(\lambda)$) relative to that of the fused silica substrate ($I_{substrate}(\lambda)$) derived from the original transmitted light signals (provided in the Appendix). Three wavelength intervals are discussed below: the UV range (250 - 400 nm), where absorption occurred; the PAR range (400 - 700 nm), where photoluminescence was observed; and the NIR range (700 - 750 nm), where neither absorption nor photoluminescence took place.

The transmittance values in the 250 - 400 nm range were generally below unity due to waveguiding, backward scattering, and UV absorption. This range of data was converted into the coating's absorption spectrum $A_{coating}(\lambda)$ in Fig. 4 and discussed later. In the 400 - 700 nm range of the transmittance spectra, a pronounced emission from the luminescent coatings was clearly observed. A transmittance value exceeding unity indicates that additional photosynthetically active radiation (PAR) enters the greenhouse as a result of luminescence generated through UV-to-PAR conversion. This effect was particularly prominent because the deuterium lamp emitted a disproportionately high amount of UV radiation relative to the AM1.5 solar spectrum. To correct for this, the AM1.5 solar spectrum was applied in the PAR Enhancement calculation, effectively removing the influence of the lamp features as explained by $I_{solar}(\lambda)$ in Eq. (3). The use of a deuterium lamp improves the accuracy of UV absorption measurements and PAR Enhancement, while our calculation method conveniently allows the use of any lamp type. The dips at 650 and 660 nm resulted from intense lamp spectral peaks that are difficult to correct for. In the NIR range,

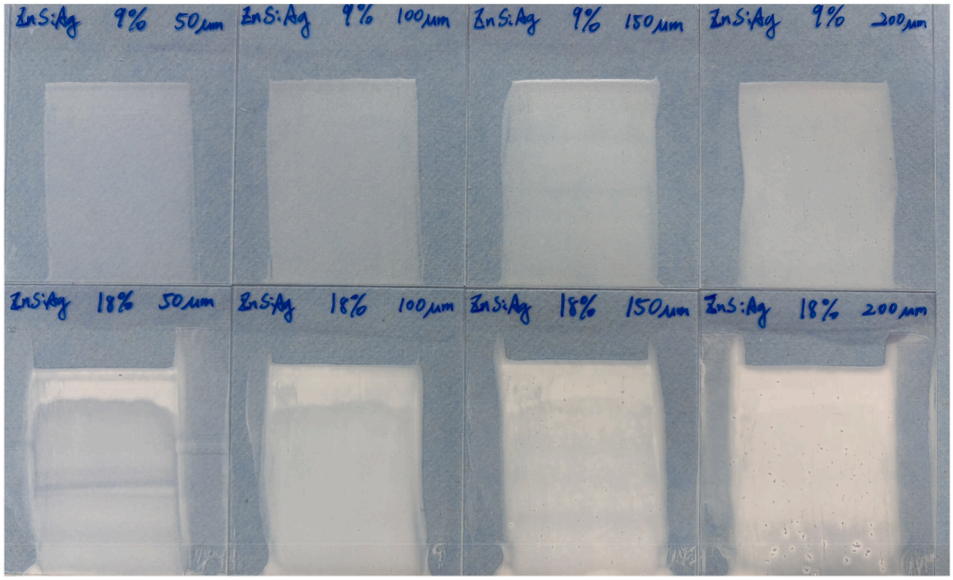

Fig. 1. Final appearance of ZnS:Ag coatings.

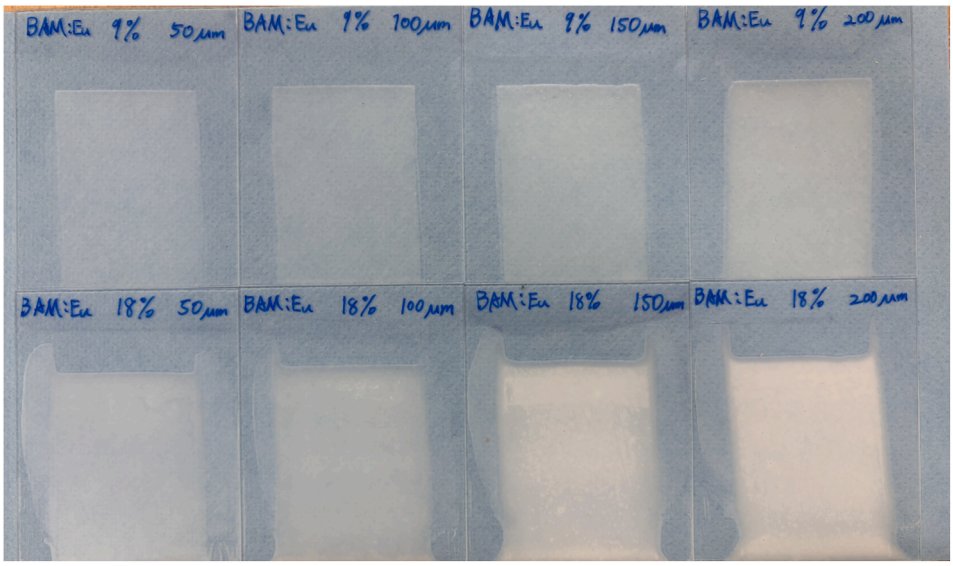

Fig. 2. Final appearance of BAM:Eu coatings.

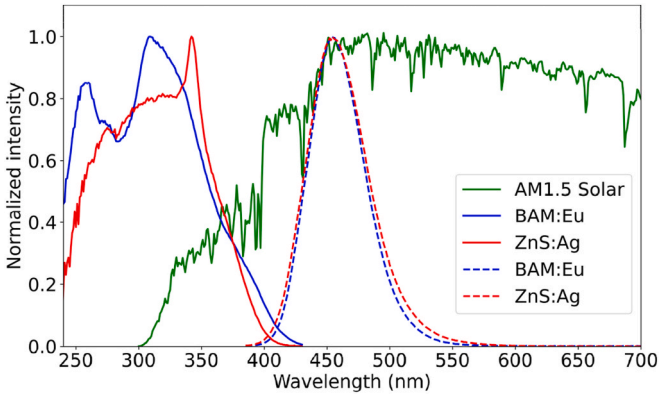

Fig. 3. Normalized photoluminescence excitation (solid lines) and photoluminescence (dashed lines) spectra with AM1.5 solar spectrum.

transmittance was governed by backward scattering and waveguiding effects, with no contribution from either emission or absorption as discussed before. The C_{Ref} value was determined by averaging the transmittance of the sample relative to the substrate over this spectral region.

Fig. 5 presents the C_{Ref} values of all samples. A small C_{Ref} value indicates substantial backward scattering and waveguiding effects in the coating. Both backward scattering and waveguiding effects lead to a general reduction in the incident photon flux of PAR entering a greenhouse. Moreover, a small C_{Ref} value may indirectly reduce PAR Enhancement because fewer incident UV photons remain available for absorption and conversion due to the backward scattering and waveguiding effects.

Both increased coating thickness and higher particle loading result in a smaller C_{Ref}, demonstrating.

Enhanced scattering and waveguiding effects. ZnS:Ag coatings showed a smaller C_{Ref} compared to the oxide-based phosphor BAM:Eu, indicating that backward scattering and waveguiding effect were more pronounced in ZnS:Ag coatings. This difference is primarily attributed to the refractive-index contrast between the phosphor particles and the surrounding medium: ZnS has a higher refractive index ($n \approx 2.3$) than BAM:Eu ($n \approx 1.7$), which increases reflection at particle–polymer interfaces and thereby strengthens scattering. In a simplified picture, the Fresnel relations predict higher interfacial reflectance for larger refractive index mismatch, leading to more frequent changes in photon propagation direction and a higher probability of photons being redirected backward or guided laterally within the coating. The influence of refractive index is further discussed together with T_{HEM} in Section 3.3. All no-phosphor reference coatings showed C_{Ref} values between 0.99 and 1.00, consistent with their high optical transparency in the absence of scattering particles.

Fig. 6 shows the absorption spectra of all coatings derived from Eq. (1). ZnS:Ag coatings exhibited a step like absorption edge near 340 nm, whereas BAM:Eu displayed an absorption band around 310 nm. These features are consistent with the corresponding PLE spectra of the phosphors in Fig. 3. The coating's absorption strength increased as both the particle loading and coating thickness increased.

Across all coating formulations, ZnS:Ag exhibited only a slightly higher absorption strength than BAM:Eu. Despite ZnS:Ag having a substantially higher absorption coefficient ($10^4 \sim 10^5$ cm^{-1}) due to the CB→VB transitions, up to two orders of magnitude higher than Eu^{2+} 4f→5d transitions in BAM ($10^3 \sim 10^4$ cm^{-1}), the measured absorption of ZnS:Ag coatings was only slightly higher than that of BAM:Eu coatings. The most plausible explanation lies in the diameter of the used phosphor particles. Although BAM:Eu has a lower intrinsic absorption coefficient, its particle size of 4 μm provides a sufficiently long optical path allowing UV photons to be absorbed, leading to a high absorption %.

In Eq. (3), the absorption spectrum $A_{coating}(\lambda)$ of each luminescent coating is applied to the AM1.5 solar spectrum $I_{solar}(\lambda)$ to calculate the total number of solar UV photons absorbed within the 280 - 400 nm range which is the more relevant absorption quantity when considering greenhouse applications. To demonstrate how much UV light was absorbed by each coating, the ratio of absorbed UV photons to the total incident UV photons in the.

AM1.5 spectrum, $A_{coating}(\lambda)$ was calculated according to Eq. (4) below and shown in Fig. 7 a.

$$A_{solar}(\%) = \frac{\int_{250}^{400} \left[A_{coating}(\lambda) * I_{solar}(\lambda)\right] d\lambda}{\int_{250}^{400} I_{solar}(\lambda) d\lambda} \quad (4)$$

In general, ZnS:Ag coatings absorbed more solar UV photons than BAM:Eu coatings at the same particle mass loading. The absorption strength clearly influenced the amount of absorbed UV photons. In addition, the shape of the absorption spectrum also played a role in the amount of total absorbed UV photons. The absorption spectrum of BAM:Eu coatings showed a peak at 310 nm and then decreased toward longer wavelengths, while ZnS:Ag coatings showed a step-like feature until 340 nm and gradually decreased toward longer wavelengths. Since the

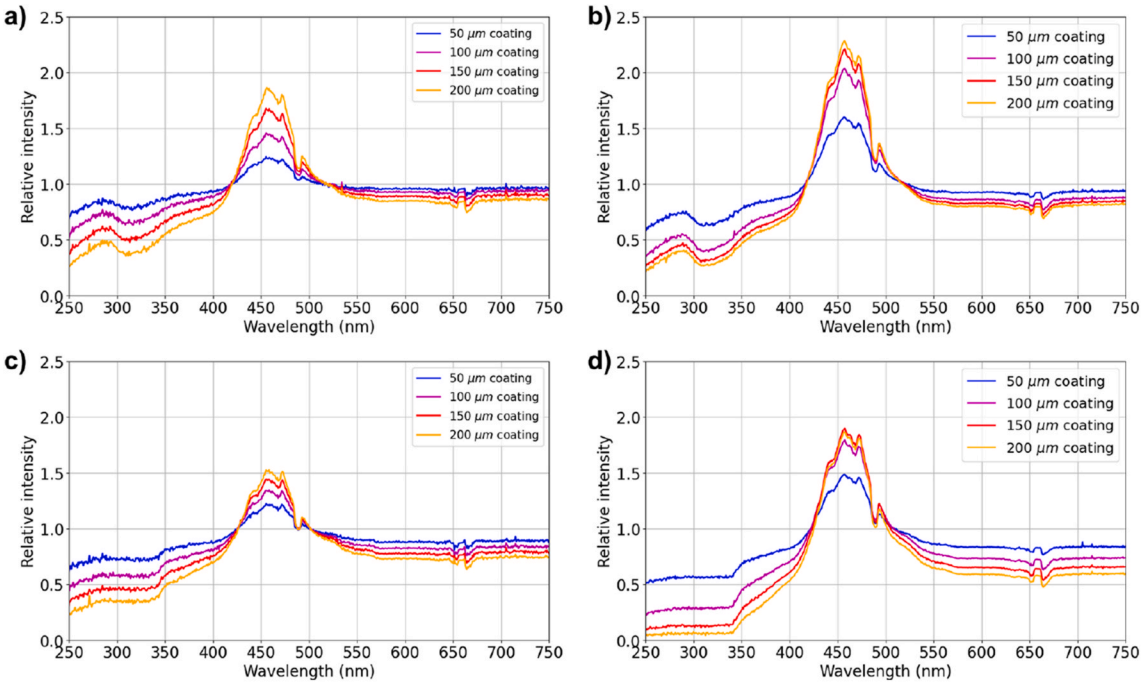

Fig. 4. The transmittance spectrum of all samples, relative to the substate, measured using an integrating sphere. a) BAM:Eu 9 mass% with various coating thickness. b) BAM:Eu 18 mass% with various coating thickness. c) ZnS:Ag 9 mass% with various coating thickness. d) ZnS:Ag 18 mass% with various coating thickness.

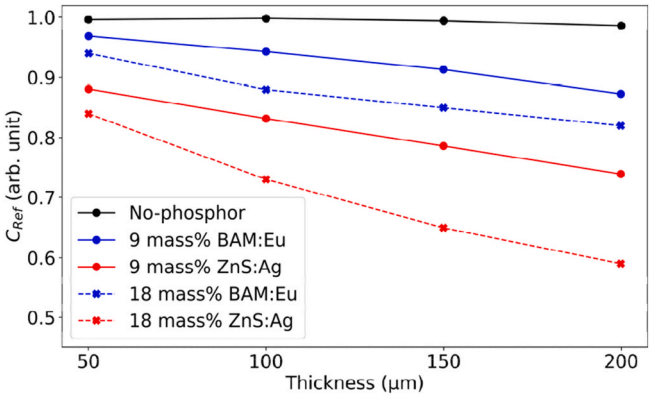

Fig. 5. C_{Ref} of all coating samples.

UV photon flux in the AM1.5 solar spectrum is not uniform, as illustrated in Fig. 6, this spectral feature also contributed to the higher solar UV absorption in ZnS:Ag coatings compared to BAM:Eu coatings. Therefore, coatings that maintain a high absorption across the entire solar UV range or exhibit stronger absorption at longer UV wavelengths (close to 400 nm) are more effective at capturing available UV photons, ultimately resulting in greater total UV absorption and enhancing PAR generation.

The number of luminescence-generated PAR photons entering the greenhouse per absorbed UV photon, denoted as $\eta_{coating}$, depends primarily on the photoluminescence quantum yield (PLQY), which is an intrinsic property of each phosphor and does not vary with particle loading or coating thickness. Under the assumption of isotropic emission, only 50% of the emitted photons are directed toward the interior of the greenhouse, while the remaining 50% escape outward, leaving the greenhouse. Under these idealized conditions, $\eta_{coating}$ should not exceed half the PLQY, which results in 46% for BAM:Eu coatings and 43% for ZnS:Ag coatings.

As shown in Fig. 7b, $\eta_{coating}$ exhibits only a weak dependence on coating thickness, particularly for ZnS:Ag coatings, but increases markedly with particle loading. In the 9 mass% series, both phosphors showed similar $\eta_{coating}$ values in the range of 20-25%. However, in the 18 mass% series, both BAM:Eu and ZnS:Ag coatings approached the theoretical limit of $\eta_{coating}$ at 200 μm, reaching 40% for BAM:Eu and 37% for ZnS:Ag. The increase in $\eta_{coating}$ observed at a higher particle mass loading may be partly attributed to the configuration of the measurement setup. When the coating sample covers the port of the integrating sphere, photons that have entered the sphere after transmitting through the coating are retained within the sphere due to back-reflection at the coating, thereby enhancing the detected signal. Coatings that exhibit stronger backward scattering can further increase this internal retention, which is consistent with the trend in C_{Ref} values observed in Fig. 5. It should be noted that this "photon retention" contribution is specific to the integrating sphere configuration and may lead to a modest overestimation of $\eta_{coating}$ for highly scattering coatings, because a fraction of photons that would otherwise escape the detection geometry can be redirected into the sphere and collected. In practical greenhouse operation, the space beneath the coating is not an ideal reflective cavity; consequently, backward scattering at the coating is expected to primarily reduce the net transmitted PAR flux rather than enhance photon collection in the greenhouse. Therefore, $\eta_{coating}$ is interpreted here mainly as an intrinsic conversion metric, whereas application-relevant performance must be assessed by jointly considering $\eta_{coating}$ with other performance indicators.

Although $\eta_{coating}$ was primarily determined by the PLQY of the phosphors used, the result indicated it can be influenced by formulation parameters such as particle loading and thickness. Since a higher $\eta_{coating}$ directly contributes to greater PAR Enhancement, optimizing $\eta_{coating}$ is essential for maximizing the overall performance of the coating.

Finally, the PAR Enhancement values are presented in Fig. 8. PAR Enhancement increased with both coating thickness and particle loading. At 9 mass% loading, ZnS:Ag coatings exhibited only slightly higher PAR Enhancement than BAM:Eu. Both ZnS:Ag and BAM:Eu coatings reached 0.5% PAR Enhancement at 200 μm thickness. At 18 mass% loading, ZnS:Ag coatings again showed a larger PAR Enhancement than the BAM:Eu coatings. Both phosphors achieved the highest PAR Enhancement values at 200 μm, which was 1.0% for BAM:Eu and

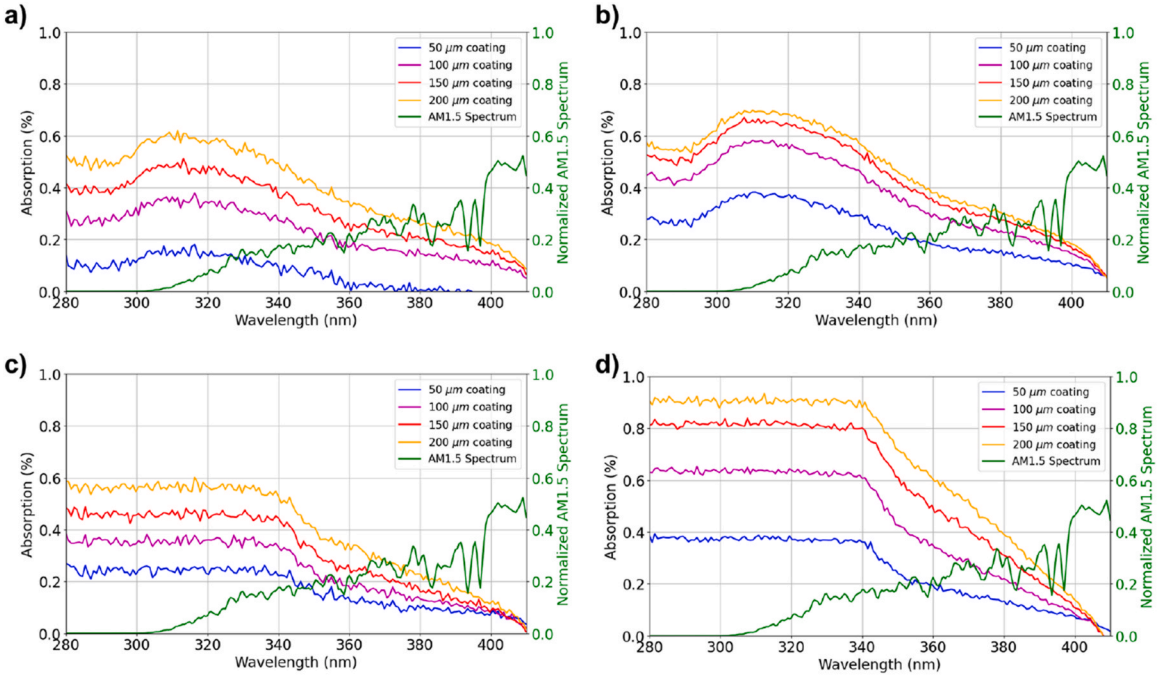

Fig. 6. The absorption spectrum of all samples, derived from the transmitted light signals in Fig. 3. The green curve is the normalized AM1.5 solar spectrum. a) BAM:Eu 9 mass% coatings with various thickness. b) BAM:Eu 18 mass% coatings with various thickness. c) ZnS:Ag 9 mass% coatings with various thickness. d) ZnS:Ag 18 mass% coatings with various thickness. (For interpretation of the references to colour in this figure legend, the reader is referred to the Web version of this article.)

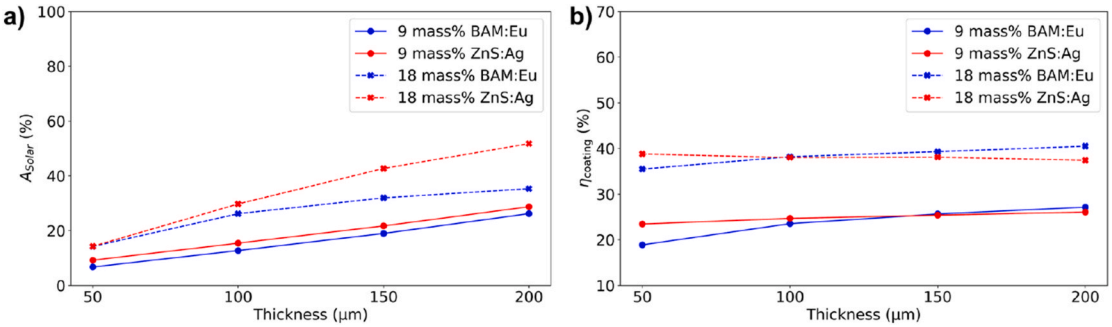

Fig. 7. a) The absorption of total UV photon, A_{solar}(%), within 280 - 400 nm range in AM1.5 solar spectrum of all coating samples. b) UV-to-PAR conversion efficiency $\eta_{coating}$ of all coating samples.

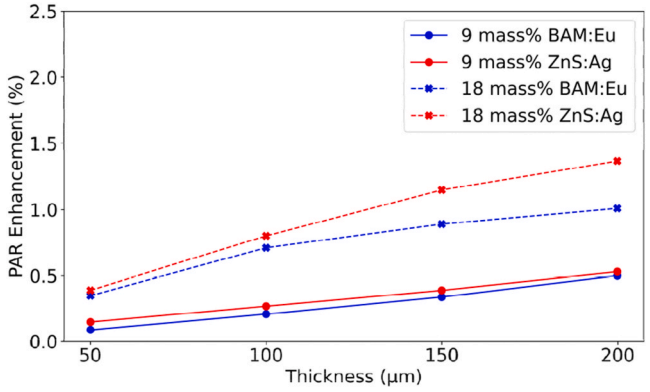

Fig. 8. PAR Enhancement of all coating samples.

1.3% for ZnS:Ag.

Despite the strong backward scattering effect for ZnS:Ag coatings, as indicated by C_{Ref}, and its slightly lower PLQY, the PAR Enhancement was higher due to its higher UV absorption as shown in Fig. 7a.

These results demonstrate that both $\eta_{coating}$ and the total UV absorption are primary factors controlling PAR Enhancement. The UV absorption can be tuned by adjusting coating thickness and particle loading, while $\eta_{coating}$ is influenced primarily by the particle mass loading.

3.3. *Hemispherical light transmittance T_{HEM} and diffuse reflection*

The T_{HEM} of luminescent coatings with 9 mass% and 18 mass% particle loading is presented in Fig. 9a. For all luminescent coating series, including the no-phosphor series, T_{HEM} decreased with increasing thickness and particle loading. The attenuation of the light signal is a combined effect of the backward scattering and waveguiding in the polymer matrix and substrate. Needless to say, PAR enhancement values by luminescence presented in Fig. 8 are far smaller than the losses by backward scattering evidenced by the T_{HEM} values presented in Fig. 9a.

BAM:Eu coatings showed higher T_{HEM} values than ZnS:Ag coatings at the same thickness and loading, meaning more PAR light penetrating through the coating into the greenhouse. This difference can be again explained by the refractive index of the phosphors. BAM:Eu, an oxide

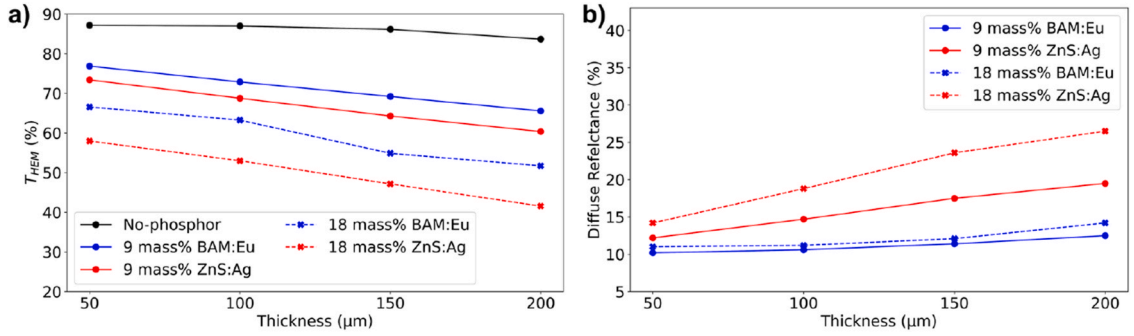

Fig. 9. a) Hemispherical light transmittance (T_{HEM}) of all coating samples. b) Diffuse reflectance of all coating samples.

material, has a lower refractive index (n ≈ 1.7), while ZnS:Ag, a sulphide material, has a higher value (n ≈ 2.3). As discussed when presenting C_{Ref} values, a larger refractive index results in a greater reflectance as predicted by the Fresnel equation.

To verify that the optical losses were primarily caused by backward scattering, diffuse reflectance measurements were performed on the coatings and presented in Fig. 9b. Unlike C_{Ref}, which accounts for light loss from both backward scattering and waveguiding effects, diffuse reflectance captures only the backward scattered light from the sample. As shown, diffuse reflectance increased with both coating thickness and particle loading. The generally higher reflectance observed in ZnS:Ag coatings compared to BAM:Eu coatings supports the conclusion that the refractive index of the phosphor plays a significant role in hemispherical light transmittance. Overall, the results demonstrated that particle loading, coating thickness, and refractive index all influence losses by scattering and consequently affect the hemispherical light transmittance of the coating.

3.4. General discussion

Incorporating 8 μm ZnS:Ag phosphor into a 200 μm-thick coating at a particle loading of 18 mass% increases the PAR level by 1.3%. The theoretical limit of 3.5% could be approached by engineering the coating formulation, for example, by increasing the coating thickness and/or phosphor loading. It should be noted that such modifications would likely increase cost, complicate practical implementation, and further reduce PAR transmittance.

The concept of spectral conversion in the greenhouse environment is intuitively beneficial for enhancing plant growth and increasing crop yield, but the potential gain from PAR-emitting coating is counteracted by light losses due to backward scattering at the coating. In our coating, such losses lowered the hemispherical light transmittance by as much as 45%. It is important to note that phosphors with a higher refractive index, such as ZnS (n ≈ 2.3), exhibited a larger scattering efficiency, lowering T_{HEM} to a larger extent than BAM:Eu (n ≈ 1.7). Consequently, phosphors with similar or even higher refractive index that have been suggested for spectral conversion purposes such as (oxy)sulphides and (oxy)nitrides, including Ca(Sr)ZnOS:Eu^{2+}, (Ca,Sr)S:Eu^{2+}, and Ba_2ZnS_3:Eu^{2+}, are less suitable.

Reducing particles' backward scattering efficiency is therefore indispensable and could be achieved by employing larger particles that favour forward scattering as predicted by Mie theory, or particles with a radius much smaller than the wavelength of light [34]. Although this approach is conceptually sound, reducing scattering by changing radius also reduces absorption, which necessitates a higher particle density or coating thickness, both of which can reintroduce scattering losses. The true scientific challenge is to significantly reduce scattering strength without affecting or preferably even increasing absorption strength. Despite the fact that scattering significantly decreases PAR transmittance, scattering by itself, formally quantified as "hortiscatter," can also promote plant growth because it generates a more even light distribution on leaves [6,7]. Future research should explicitly evaluate the combined effects of hortiscatter and hemispherical light transmittance, including PAR Enhancement, on crop yield improvement.

Phosphors selected for greenhouse applications should exhibit a high PLQY, a low refractive index to minimize scattering losses, and sufficient chemical stability under operating conditions. Accordingly, a practical spectral-conversion greenhouse coating should combine low backward scattering with high PAR transmittance, strong UV absorption, and high UV-to-PAR conversion efficiency, thereby increasing the PAR photon supply in the greenhouse without reducing the baseline transmitted PAR from sunlight.

4. Conclusion

A series of luminescent coatings based on two commercial UV-absorbing, PAR-emitting phosphors (ZnS:Ag and $BaMgAl_{10}O_{17}$:Eu^{2+}) was fabricated to assess their suitability for greenhouse spectral conversion. Key optical performance metrics, including UV absorption and UV-to-PAR conversion efficiency, hemispherical light transmittance (T_{HEM}), and PAR Enhancement, were systematically quantified as a function of coating thickness and phosphor loading.

The results show that particle based spectral conversion coatings can provide measurable PAR enhancement inside the greenhouse, reaching up to 1.3% for a 200 μm coating containing 18 mass% ZnS:Ag. However, pronounced backward scattering, consistent with the high refractive index of ZnS, substantially reduced T_{HEM} and thus the total transmitted PAR photon flux, demonstrating that scattering losses can counteract the benefits of spectral conversion. By comparison, the activator-absorption phosphor $BaMgAl_{10}O_{17}$:Eu^{2+} achieved a slightly lower PAR enhancement (1.0%) while exhibiting a smaller reduction in hemispherical transmittance, attributable to its lower refractive index and correspondingly weaker backward scattering.

Overall, this work provides an experimental quantification of both the optical gains (PAR Enhancement) and losses (transmittance reduction and backward scattering) associated with UV-to-PAR luminescent greenhouse coatings. The presented measurement workflow and performance indicators offer a practical framework for future studies to assess spectral conversion coatings under application-relevant conditions and to guide phosphor/coating design toward simultaneously high UV absorption and conversion efficiency with minimal scattering-induced PAR losses.

CRediT authorship contribution statement

Chun-Ting Cho: Conceptualization, Data curation, Formal analysis, Investigation, Methodology, Project administration, Visualization, Writing – original draft. **Erik van der Kolk:** Conceptualization, Funding acquisition, Project administration, Resources, Supervision, Writing – review & editing.

Declaration of competing interest

The authors declare that they have no known competing financial interests or personal relationships that could have appeared to influence the work reported in this paper.

Acknowledgement

This research received funding from the Dutch Research Council (NWO) in the framework of the Science PPP Fund for the top sectors and from the Ministry of Economic Affairs in the framework of the "PPS-Toeslagregeling".

Appendix A. Supplementary data

Supplementary data to this article can be found online at https://doi.org/10.1016/j.optmat.2026.117945.

Data availability

The data supporting this article have been included as part of the Supplementary Information.

References

[1] Food Security Information Network, FSIN and global network against food crises, tech. rep. https://www.fsinplatform.org/report/global-report-food-crises-2024/, 2024.
[2] I. Mirón, C. Linares, J. Díaz, The influence of climate change on food production and food safety, Environ. Res. 216 (2023) 1–6, https://doi.org/10.1016/j.envres.2022.114674.
[3] U. Mc Carthy, I. Uysal, R. Badia-Melis, S. Mercier, C. O'Donnell, A. Ktenioudaki, Corrigendum to 'global food security – issues, challenges and technological solutions, Trends Food Sci. Technol. 123 (2022) 404, https://doi.org/10.1016/j.tifs.2022.03.029.
[4] D. Zhou, H. Meinke, M. Wilson, L. Marcelis, E. Heuvelink, Towards delivering on the sustainable development goals in greenhouse production systems, Resour. Conserv. Recycl. 169 (2021), https://doi.org/10.1016/j.resconrec.2020.105379.
[5] P. Zabel, M. Bamsey, D. Schubert, M. Tajmar, Review and analysis of over 40 years of space plant growth systems, Life Sci. Space Res. 10 (2016) 1–16, https://doi.org/10.1016/j.lssr.2016.06.004.
[6] E. Victoria, N. Romero, B. van Breugel, C. Stanghellini, S. Hemming, Can extreme light diffusion still increase crop growth in greenhouses? Acta Hortic. 1423 (2025) 79–86, https://doi.org/10.17660/ActaHortic.2025.1423.11.
[7] G. van Steekelenburg, S. Hemming, E. Kaiser, E. Heuvelink, Quantifying the effects of hortiscatter in greenhouse cover materials on crop yield, Acta Hortic. 1423 (2025) 87–94, https://doi.org/10.17660/ActaHortic.2025.1423.12.
[8] M. Teitel, H. Vitoshkin, F. Geoola, S. Karlsson, N. Stahl, Greenhouse and screenhouse cover materials: literature review and industry perspective, Acta Hortic. 1227 (2018) 31–44, https://doi.org/10.17660/ActaHortic.2018.1227.4.
[9] G. Giacomelli, W. Roberts, Greenhouse covering systems, HortTechnology 3 (1993) 50–58.
[10] C. Maraveas, Environmental sustainability of greenhouse covering materials, Sustainability 11 (2019), https://doi.org/10.3390/su11216129.
[11] K. Mishra, C. Stanghellini, S. Hemming, Technology and materials for passive manipulation of the solar spectrum in greenhouses, Adv. Sustain. Syst. 7 (2023), https://doi.org/10.1002/adsu.202200503.
[12] H. Aldaftari, J. Okajima, A. Komiya, S. Maruyama, Radiative control through greenhouse covering materials using pigmented coatings, J. Quant. Spectrosc. Radiat. Transf. 231 (2019) 29–36, https://doi.org/10.1016/j.jqsrt.2019.04.009.15.
[13] T. Li, Y. Gao, K. Zheng, Y. Ma, D. Ding, H. Zhang, Achieving better greenhouse effect than glass: visibly transparent and low emissivity metal-polymer hybrid metamaterials, Energy Environ. 5 (2019) 102–107, https://doi.org/10.30919/esee8c325.
[14] S. Hemming, T. Dueck, J. Janse, F. Van Noort, The effect of diffuse light on crops, Acta Hortic. 801 (2008) 1293–1300, https://doi.org/10.17660/ActaHortic.2008.801.158.
[15] F. Kempkes, C. Stanghellini, N.G. Victoria, M. Bruins, Effect of diffuse glass on climate and plant environment: first results from an experiment on roses, Acta Hortic. 952 (2012) 255–262, https://doi.org/10.17660/ActaHortic.2012.952.31.
[16] R. Yalçin, H. Ertürk, Improving photosynthetic efficiency using greenhouse coatings with scattering and fluorescent pigments, Mater. Res. Express 6 (2019), https://doi.org/10.1088/20531591/ab28b8.
[17] Y. Fan, Y. Zhou, Z. Qiu, S. Lian, Photoluminescent materials for solar spectral conversion greenhouse films, J. Mater. Chem. C 13 (2025) 5462–5482.
[18] S. Hemming, D. Waaijenberg, G. Bot, P. Sonneveld, F. de Zwart, T. Dueck, C. van Dijk, A. Dieleman, N. Marissen, E. van Rijssel, B. Houter, Optimaal Gebruik Van Natuurlijk Licht in De Glastuinbouw, 100, Agrotechnology & Food Innovations, 2004, p. 154.
[19] F. Hollósy, Effects of ultraviolet radiation on plant cells, Micron 33 (2002) 179–197, https://doi.org/10.1016/S0968-4328(01)00011-7.
[20] E. Kovács, Keresztes, effect of gamma and UV-B/C radiation on plant cells, Micron 33 (2002) 199–210, https://doi.org/10.1016/S0968-4328(01)00012-9.
[21] G. Nawkar, P. Maibam, J. Park, V. Sahi, S. Lee, C. Kang, UV-induced cell death in plants, Int. J. Mol. Sci. 14 (2013) 1608–1628, https://doi.org/10.3390/ijms14011608.
[22] S. Jakka, M. Silva, M. Soares, K. Pavani, Exploring the potential of Eu^{3+} and Mn^{4+}activated $LaAlO_3$ phosphors as red and far-red emitters for horticulture lighting, RSC Adv. 13 (2023) 31314–31320, https://doi.org/10.1039/d3ra03241h.
[23] C. Cho, G. Bosco, E. van der Kolk, The Potential of SiO_2:Al^{3+},Eu^{2+} Blue Phosphor Coatings in Greenhouse Application, 157, 2024, pp. 2–8.
[24] A. Shabalina, V. Kozlov, M. Paskhin, I. Popov, S. Gudkov, A mini-review of photoconversion covers for greenhouses: assessment parameters and plant experiment results, Horticulturae 11 (2025) 680, https://doi.org/10.3390/horticulturae11060680.
[25] M. Ge, Y. Yuan, S. Liu, J. Li, C. Yang, B. Du, Q. Pang, S. Li, Z. Chen, Enhancing plant photosynthesis with dual light conversion films incorporating biomass-derived carbon dots, Carbon Capture Sci. Technol. 13 (2024), https://doi.org/10.1016/j.ccst.2024.100253.
[26] S. Adachi, S. Ozaki 1, Optical constants of cubic ZnS, Jpn. J. Appl. Phys. 32 (1993) 5008–5013, https://doi.org/10.1143/JJAP.32.5008.16.
[27] A. Rocha, L. Andrade, S. Lima, A. Farias, A. Bento, M. Baesso, Y. Guyot, G. Boulon, Tunable color temperature of Ce^{3+}/$Eu^{2+,3+}$ co-doped low silica aluminosilicate glasses for white lighting, Opt. Express 20 (2012) 10034–10041.
[28] Z. Ye, L. Kong, F. Chen, Z. Chen, Y. Lin, C. Liu, A comparative study of photocatalytic activity of ZnS photocatalyst for degradation of various dyes, Optik 164 (2018) 345–354.
[29] C. Gueymard, D. Myers, K. Emery, Proposed reference irradiance spectra for solar energy systems testing, Sol. Energy 73 (2002) 443–467, https://doi.org/10.1016/S0038-092X(03)00005-7.
[30] J. Zhang, Z. Zhang, Z. Tang, Y. Tao, X. Long, Luminescent Properties of the $BaMgAl_{10}O_{17}$:Eu^{2+}, M^{3+} (M = Nd, Er) phosphor in the VUV Region, Chem. Mater. 14 (2002) 3005–3008.
[31] V. Singh, R. Chakradhar, J. Rao, H. Kwak, Photoluminescence and EPR studies of $BaMgAl_{10}O_{17}$:Eu^{2+} phosphor with blue-emission synthesized by the solution combustion method, J. Lumin. 131 (2011) 1714–1718, https://doi.org/10.1016/j.jlumin.2011.03.030.
[32] Y. Uehara, Electronic structure of luminescence center of zns:ag phosphors, J. Chem. Phys. 62 (1974) 2982–2994, https://doi.org/10.1063/1.430903.
[33] G. Blasse, B. Grabmaier, Luminescent Materials, Springer Berlin, Heidelberg, 1994.
[34] J. Meyer-Arendt, Introduction to Classical and Modern Optics, Prentice Hall, Englewood Cliff, NJ, 1989.